

September 10, 2018

Radiative Penguin Decays at e^+e^- Colliders

GERALD EIGEN ¹

(REPRESENTING THE *BABAR* COLLABORATION)

Department of Physics

University of Bergen, N-5007 Bergen, NORWAY

In this review, the most recent results of the radiative decays $B \rightarrow X_s \gamma$, $B \rightarrow K^{(*)} \ell^+ \ell^-$ and $B \rightarrow \pi/\eta \ell^+ \ell^-$ at e^+e^- colliders are discussed. The new, most precise CP asymmetry measurements in $B \rightarrow X_s \gamma$ from *BABAR* are presented together with branching fractions and photon energy moments. For $B \rightarrow K^{(*)} \ell^+ \ell^-$ modes, B factory results on partial branching fractions, rate asymmetries and angular observables are combined with measurements from CDF and the LHC experiments. The first branching fraction upper limits for $B \rightarrow \eta \ell^+ \ell^-$ are shown along with updated upper limits of $B \rightarrow \pi \ell^+ \ell^-$ branching fractions.

PRESENTED AT

Flavor Physics and CP Violation
Buzios, Rio, Brasil, May 19–24, 2013

¹Work supported by the Norwegian Research Council.

1 Introduction

The decays $B \rightarrow X_{s(d)}\gamma$ and $B \rightarrow X_{s(d)}\ell^+\ell^-$, where $\ell^+\ell^-$ is e^+e^- or $\mu^+\mu^-$, are flavor-changing neutral-current processes that are forbidden in the Standard Model (SM) at tree level. They occur in higher-order processes and are described by an effective Hamiltonian that factorizes short-distance contributions in terms of scale-dependent Wilson coefficients $C_i(\mu)$ from long-distance effects expressed by local four-fermion operators \mathcal{O}_i that define hadronic matrix elements,

$$H_{eff} = \frac{4G_F}{\sqrt{2}} \sum_i C_i(\mu)\mathcal{O}_i. \quad (1)$$

While Wilson coefficients are calculable perturbatively, the calculation of the hadronic matrix elements requires non-perturbative methods such as the heavy quark expansion [1, 2, 3, 4].

Figure 1 shows the lowest order diagrams. In the $B \rightarrow X_{s(d)}\gamma$ decay, the electromagnetic penguin loop dominates. The short-distance part is expressed by the effective Wilson coefficient C_7^{eff} . Through operator mixing at higher orders, the chromo-magnetic penguin enters whose short distance part is parameterized by C_8^{eff} . In $B \rightarrow X_{s(d)}\ell^+\ell^-$ modes, the Z penguin and the WW box diagram contribute in addition. Their short-distance parts are parametrized in terms of C_9^{eff} (vector current part) and C_{10}^{eff} (axial-vector current part). Physics beyond the SM introduces new loops and box diagrams with new particles (*e.g.* charged Higgs boson, supersymmetric particles) as shown in Fig. 2. Such contributions modify the Wilson coefficients and may introduce new diagrams with scalar and pseudoscalar current interactions and in turn new Wilson coefficients, C_S and C_P . To determine C_7^{eff} , C_8^{eff} , C_9^{eff} and C_{10}^{eff} precisely, we need to measure many observables in several radiative decays. These rare decays can potentially probe new physics at a scale of a few TeV.

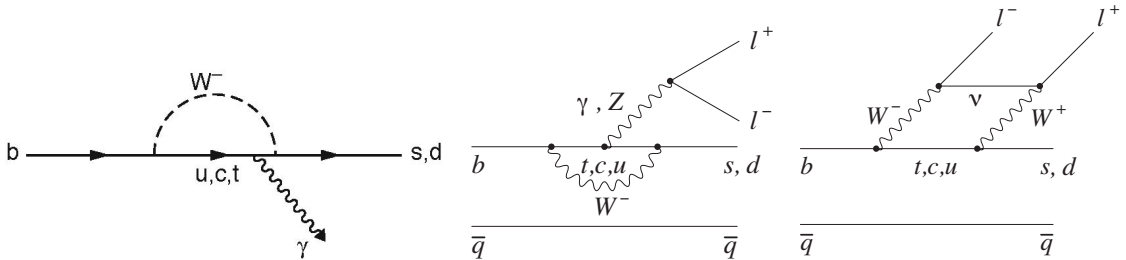


Figure 1: Lowest-order diagrams for $B \rightarrow X_{s(d)}\gamma$ (left) and $B \rightarrow X_{s(d)}\ell^+\ell^-$ (middle, right).

We present herein new *BABAR* measurements of the direct CP asymmetry in $B \rightarrow X_s\gamma$ using a semi-inclusive analysis and determine the ratio of Wilson coefficients $\mathcal{I}m(C_8^{eff}/C_7^{eff})$. In addition, we summarize the status of partial branching

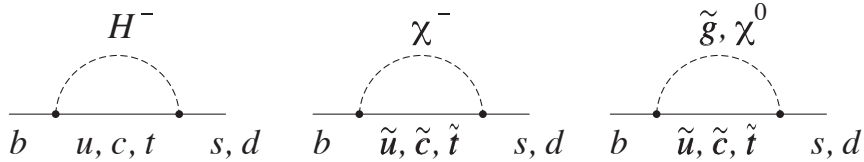


Figure 2: Examples of new physics processes.

fractions, photon energy spectra, photon energy moments and CP asymmetries from e^+e^- colliders for fully inclusive and semi-inclusive $B \rightarrow X_s\gamma$ analyses. We determine the b quark mass m_b and its kinetic energy μ_π^2 in the kinetic and shape function models. We review the status of branching fractions, rate asymmetries and angular observables for $B \rightarrow K^{(*)}\ell^+\ell^-$ modes. Finally, we present a new *BABAR* search for $B \rightarrow \pi\ell^+\ell^-$ modes and a first search for $B \rightarrow \eta\ell^+\ell^-$ modes. *BABAR* performs all analyses blinded.

2 Study of $B \rightarrow X_s\gamma$

In the SM, the $B \rightarrow X_s\gamma$ branching fraction is calculated at next-to-next-to-leading order (up to four loops) yielding $\mathcal{B}(B \rightarrow X_s\gamma) = (3.14 \pm 0.22) \times 10^{-4}$ for photon energies $E_\gamma^* > 1.6$ GeV [5, 6, 7]. For larger minimum values of E_γ^* , the prediction depends on the shape of the E_γ^* spectrum, which is modeled in terms of a shape function that depends on the Fermi motion of the b quark inside the B meson and thus on the b quark mass. Since the shape function is expected to be similar to that used to determine the lepton-energy spectrum in $B \rightarrow X_u\ell\nu$, precision measurements of the E_γ^* spectrum are helpful for the determination of V_{ub} . The measurement of $\mathcal{B}(B \rightarrow X_s\gamma)$ provides constraints on the charged Higgs mass m_{H^\pm} .

Experimentally, the challenge is to extract the E_γ^* signal from photon background copiously produced in π^0 decays in $q\bar{q}$ continuum* and $B\bar{B}$ processes that increases exponentially with smaller photon energy. We use three different strategies to suppress these backgrounds: i) an inclusive analysis with a lepton tag, ii) a semi-inclusive analysis and iii) an inclusive analysis with a fully reconstructed B meson. Herein, we present results of the first two strategies.

2.1 Fully Inclusive $B \rightarrow X_s\gamma$ Analysis

Using a sample of 384×10^6 $B\bar{B}$ events, *BABAR* measured total and partial branching fractions, photon energy moments and the $B \rightarrow X_{s+d}\gamma$ CP asymmetry in a fully inclusive analysis [8, 9]. To suppress $e^+e^- \rightarrow q\bar{q}$ continuum and $B\bar{B}$ backgrounds, we

*q refers to u, d, s and c

tag the recoiling B meson in semileptonic decays and use optimized π^0 and η vetoes, missing energy requirements and the output of two neural networks (NN). For a signal efficiency of 2.5%, the efficiency for accepting continuum ($B\bar{B}$) background is reduced to 5×10^{-6} (1.3×10^{-4}). We estimate the residual continuum background by studying data taken 40 MeV below the $\Upsilon(4S)$ peak. Figure 3 (left) shows the $B \rightarrow X_s \gamma$ partial branching fraction after background subtraction and corrections for efficiency, resolution effects and Doppler smearing. For comparison, we show the predicted E_γ^* spectrum in the kinetic scheme [10, 11] using HFAG world averages [12] for the shape function parameters. For $E_\gamma^* > 1.8$ GeV, $BABAR$ measures a total branching fraction of $\mathcal{B}(B \rightarrow X_S \gamma) = (3.21 \pm 0.15_{stat} \pm 0.29_{sys} \pm 0.08_{model}) \times 10^{-4}$, where uncertainties are statistical, systematic and from model dependence, respectively. This is in good agreement with previous measurements [13, 14, 15]. After extrapolation to $E_\gamma > 1.6$ GeV, the branching fraction increases to $\mathcal{B}(B \rightarrow X_S \gamma) = (3.31 \pm 0.16_{stat} \pm 0.30_{sys} \pm 0.09_{model}) \times 10^{-4}$, which is still in good agreement with the SM prediction. We use this result to constrain new physics in the type II two-Higgs doublet model [5, 16, 17] excluding $m_{H^\pm} < 327$ GeV/ c^2 at 95% confidence level (CL) independent of $\tan\beta$. Recent $BABAR$ results on $\mathcal{B}(B \rightarrow D^{(*)}\tau\nu)$, however, are in conflict with both the SM and the type II Higgs doublet model at the 3σ level [18, 19].

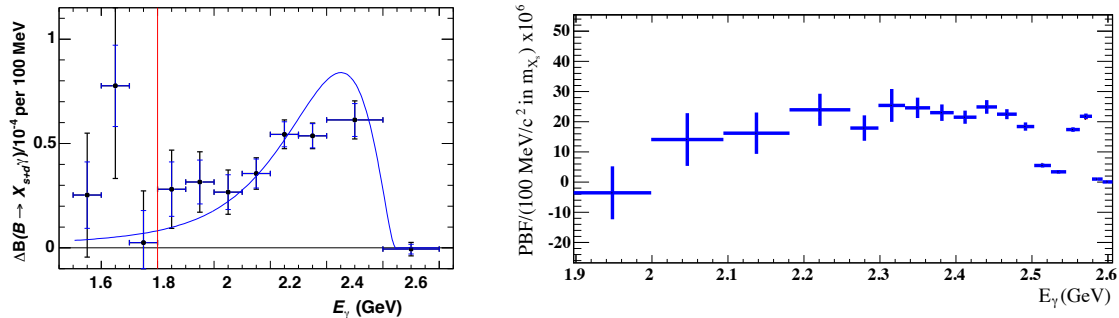


Figure 3: Partial branching fraction versus E_γ^* measured in a fully inclusive analysis (left) and for the sum of exclusive modes (right). Error bars (left) show statistical and total uncertainties. The solid curve shows a prediction for the kinetic scheme with HFAG averages [12]. The vertical bar separates signal from the control region. Errors bars (right) show total uncertainties.

For $E_\gamma^* > 1.8$ GeV, $BABAR$ measured energy moments of $\langle E_\gamma \rangle = (2.267 \pm 0.019_{stat} \pm 0.032_{sys} \pm 0.003_{mod})$ GeV and $\langle (E_\gamma - \langle E_\gamma \rangle)^2 \rangle = (0.0484 \pm 0.0053_{stat} \pm 0.0077_{sys} \pm 0.0005_{mod})$ GeV² that are consistent with previous results [13, 14, 15]. where uncertainties are statistical, systematic and from model dependence, respectively.

Table 1: Determination of m_b and μ_π^2 in the kinetic-scheme [10] and shape function scheme [21] using the semi-inclusive analysis in comparison to the world average [12].

	BABAR kinetic scheme	BABAR shape function scheme	world average kinetic scheme	world average shape function scheme
m_b [GeV/ c^2]	$4.568^{+0.038}_{-0.036}$	$4.579^{+0.032}_{-0.029}$	4.560 ± 0.023	4.588 ± 0.025
μ_π^2 [GeV 2]	0.450 ± 0.054	$0.257^{+0.034}_{-0.039}$	0.453 ± 0.036	$0.189^{+0.046}_{-0.057}$

2.2 Semi-Inclusive $B \rightarrow X_s \gamma$ Analysis

Using 471 $B\bar{B}$ events in a semi-inclusive analysis, we combine 38 exclusive $B \rightarrow X_s \gamma$ final states containing a $K^{*\dagger}$ or K_S^0 and up to four pions with at most two π^0 s, $K^+ K^-$ with up to one pion, or up to one η with up to two pions [20]. We reconstruct the hadronic mass m_{X_s} in 100 MeV/ c^2 bins and calculate the photon energy by $E_\gamma = \frac{m_B^2 - m_{X_s}^2}{2m_B}$. Figure 3 (right) shows the partial branching fraction versus E_γ^* . Summing the partial branching fraction over all m_{X_s} bins yields $\mathcal{B}(B \rightarrow X_s \gamma) = (3.29 \pm 0.19_{stat} \pm 0.48_{sys}) \times 10^{-4}$ for $E_\gamma > 1.9$ GeV, which is in good agreement with the results of the inclusive analysis. We also measure the mean and variance of the photon energy spectrum, $\langle E_\gamma \rangle = (2.346 \pm 0.018^{+0.027}_{-0.022})$ GeV and $\langle (E_\gamma - \langle E_\gamma \rangle)^2 \rangle = (0.0211 \pm 0.0057^{+0.0055}_{-0.0069})$ GeV 2 for $E_\gamma > 1.9$ GeV. These results agree with the measurements of the inclusive analysis after increasing the minimum E_γ^* selection to 1.9 GeV. Note that $\langle E_\gamma \rangle$ ($\langle (E_\gamma - \langle E_\gamma \rangle)^2 \rangle$) increases (decreases) with a larger minimum E_γ^* selection. From a fit to the photon energy spectrum, we can extract the b quark mass and its kinetic energy. Table 1 summarizes the results of m_b and μ_π^2 for fits to the E_γ^* spectrum in the kinetic scheme [10] and shape function scheme [21].

Figure 4 shows a comparison of all $B \rightarrow X_s \gamma$ total branching fraction measurements after extrapolating them to a $E_\gamma^* > 1.6$ GeV selection. In addition, the HFAG average [12] and the SM prediction [7] are depicted. All $\mathcal{B}(B \rightarrow X_s \gamma)$ measurements are in good agreement with each other and with the SM prediction.

2.3 Direct CP Asymmetry

For the sum of exclusive modes, the direct CP asymmetry is defined by

$$\mathcal{A}_{CP}(B \rightarrow X_s \gamma) \equiv \frac{\mathcal{B}(\bar{B} \rightarrow \bar{X}_s \gamma) - \mathcal{B}(B \rightarrow X_s \gamma)}{\mathcal{B}(\bar{B} \rightarrow \bar{X}_s \gamma) + \mathcal{B}(B \rightarrow X_s \gamma)}. \quad (2)$$

The present world average of $\mathcal{A}_{CP} = (-0.8 \pm 2.9)\%$ is in good agreement with the SM prediction of $-0.6\% < \mathcal{A}_{CP} < 2.8\%$ at 95% CL [24]. The presently large

[†]Charge conjugation is implied throughout the article unless stated otherwise

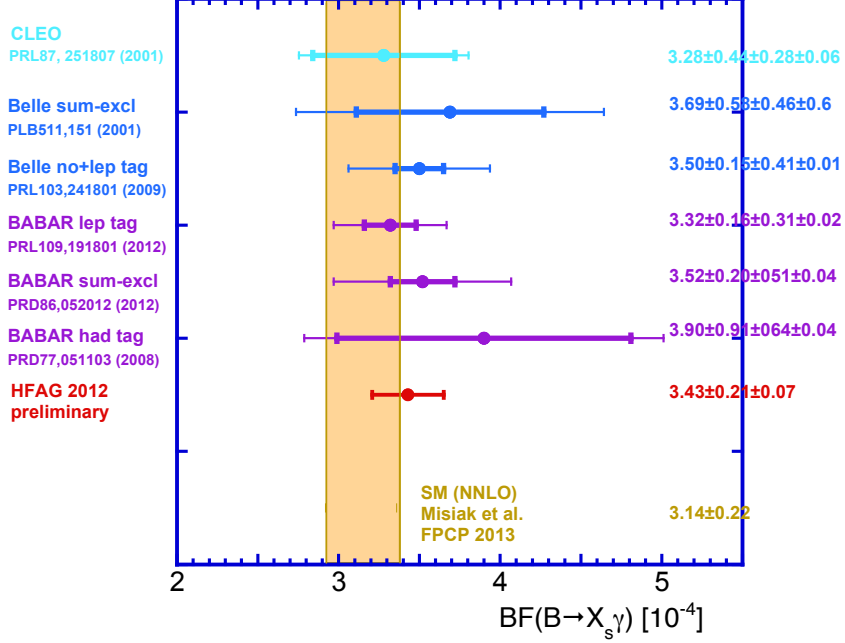


Figure 4: Comparison of $\mathcal{B}(B \rightarrow X_s \gamma)$ measurements from *BABAR* [8, 20, 22], *Belle* [14, 23] and *CLEO* [15] to the SM prediction [7] after extrapolation to $E_\gamma^* > 1.6$ GeV.

uncertainties still allow for new physics contributions, which modify C_7^{eff} . Particularly, the CP asymmetry difference between B^+ and B^0 decays, $\Delta\mathcal{A}_{CP}(B \rightarrow X_s \gamma) = \mathcal{A}_{CP}(B^+ \rightarrow X_s^+ \gamma) - \mathcal{A}_{CP}(B^0 \rightarrow X_s^0 \gamma)$, is very sensitive to new physics since it is caused by interference between the electromagnetic and the chromo-magnetic penguin diagrams in which the latter enters through higher-order corrections. Calculations yield [24]

$$\Delta\mathcal{A}_{CP}(B \rightarrow X_s \gamma) \simeq 4\pi^2 \alpha_s \frac{\bar{\Lambda}_{78}}{m_b} \mathcal{I}m \frac{C_8^{eff}}{C_7^{eff}} \simeq 0.12 \frac{\bar{\Lambda}_{78}}{100 \text{ MeV}} \mathcal{I}m \frac{C_8^{eff}}{C_7^{eff}}, \quad (3)$$

where $\bar{\Lambda}_{78}$ is the hadronic matrix element of the $\mathcal{O}_7 - \mathcal{O}_8$ interference, predicted to lie in the range $17 \text{ MeV} < \bar{\Lambda}_{78} < 190 \text{ MeV}$. In the SM, $\Delta\mathcal{A}_{CP}(B \rightarrow X_s \gamma)$ vanishes since C_7^{eff} and C_8^{eff} are real.

In a sample of 471 $B\bar{B}$ events, *BABAR* studied \mathcal{A}_{CP} and $\Delta\mathcal{A}_{CP}$ in a semi-inclusive analysis using ten B^+ and six B^0 exclusive final states.[‡] We maximize the signal

[‡] $B^+ \rightarrow K_S^0 \pi^+ \gamma, K^+ \pi^0 \gamma, K^+ \pi^+ \pi^- \gamma, K_S^0 \pi^+ \pi^0 \gamma, K^+ \pi^0 \pi^0 \gamma, K_S^0 \pi^+ \pi^- \pi^+, K^+ \pi^+ \pi^- \pi^0, K_S^0 \pi^+ \pi^0 \pi^0, K^+ \eta \gamma, K^+ K^+ K^- \gamma$ and $B^0 \rightarrow K^+ \pi^- \gamma, K^+ \pi^- \pi^0 \gamma, K^+ \pi^+ \pi^- \pi^- \gamma, K^+ \pi^- \pi^0 \pi^0 \gamma, K^+ \pi^- \eta \gamma, 3K^\pm \pi^- \gamma$.

extraction using a bagged decision tree with six input variables. This improves the efficiency considerably with respect to the standard $\Delta E = E_B^* - E_{beam}^*$ selection, where E_{beam}^* and E_B^* are the beam energy and B meson energy in the center-of-mass frame, respectively. To remove continuum background, we train a separate bagged decision tree using event shape variables. We perform an X_s mass-dependent optimization with loosely identified pions and kaons using the sensitivity $S/\sqrt{S+B}$ where S (B) is the signal (background) yield. To extract \mathcal{A}_{CP} , we fit the beam energy-constrained mass $m_{ES} = \sqrt{E_{beam}^{*2} - p_B^{*2}}$ [§] simultaneously for \bar{B} -tagged and B -tagged samples. After correcting the raw \mathcal{A}_{CP} for detector bias determined from the m_{ES} sideband below the signal region, we measure $\mathcal{A}_{CP}(B \rightarrow X_s \gamma) = (1.73 \pm 1.93_{stat} \pm 1.02_{sys})\%$, which agrees well with the SM prediction. This new measurement has the smallest uncertainty. From a simultaneous fit to B^+ and B^0 samples, we measure $\Delta\mathcal{A}_{CP}(B \rightarrow X_s \gamma) = (4.97 \pm 3.90_{stat} \pm 1.45_{sys})\%$ from which we obtain the constraint $-1.64 < \mathcal{I}m(C_8^{eff}/C_7^{eff}) < 6.52$ at 90% CL. Note, this is the first $\Delta\mathcal{A}_{CP}$ measurement and first constraint on $\mathcal{I}m(C_8^{eff}/C_7^{eff})$.

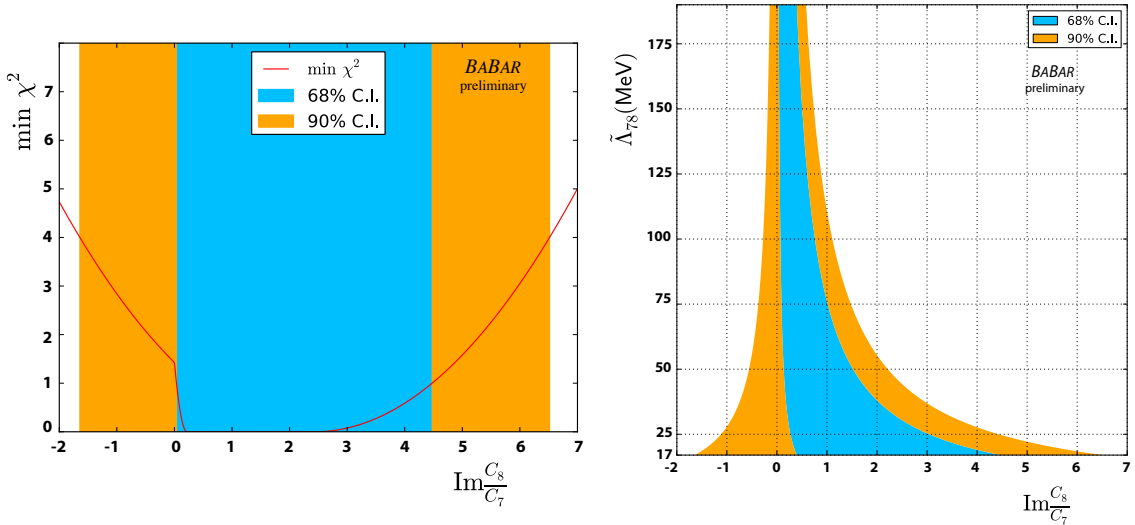


Figure 5: The $\Delta\chi^2$ function versus $\mathcal{I}m(C_8^{eff}/C_7^{eff})$ (left) and the dependence of $\bar{\Lambda}_{78}$ on $\mathcal{I}m(C_8^{eff}/C_7^{eff})$ (right). The blue dark-shaded (orange light-shaded) regions show the 68% (90%) CL intervals.

Figure 5 (left) show the $\Delta\chi^2$ of the simultaneous fit as a function of $\mathcal{I}m(C_8^{eff}/C_7^{eff})$. Figure 5 (right) shows the constraints of $\bar{\Lambda}_{78}$ as a function of $\mathcal{I}m(C_8^{eff}/C_7^{eff})$. The shape of $\Delta\chi^2$ as a function of $\mathcal{I}m(C_8^{eff}/C_7^{eff})$ is not parabolic indicating that the likelihood has a non-Gaussian shape. The reason is that $\Delta\chi^2$ is determined from all

[§] p_B^* is the B momentum in the center-of-mass frame.

possible values of $\bar{\Lambda}_{78}$. In the region $\sim 0.2 < \mathcal{I}m(C_8^{eff}/C_7^{eff}) < \sim 2.6$ a change in $\mathcal{I}m(C_8^{eff}/C_7^{eff})$ $\Delta\chi^2$ can be compensated by a change in $\bar{\Lambda}_{78}$ leaving $\Delta\chi^2$ unchanged. For positive values larger (smaller) than 2.6 (0.2), $\Delta\chi^2$ increases slowly (rapidly), since $\bar{\Lambda}_{78}$ remains nearly constant at the minimum value (increases rapidly). For negative $\mathcal{I}m(C_8^{eff}/C_7^{eff})$ values, $\bar{\Lambda}_{78}$ starts to decrease again, which leads to a change in $\Delta\chi^2$ shape.

In the fully inclusive analysis, \mathcal{A}_{CP} involves contributions from $B \rightarrow X_s\gamma$ and $B \rightarrow X_d\gamma$ that cannot be separated on an event-by-event basis. Therefore, we define \mathcal{A}_{CP} here as

$$\mathcal{A}_{CP}(B \rightarrow X_{s+d}\gamma) \equiv \frac{(\mathcal{B}(\bar{B} \rightarrow X_{s+d}\gamma) - \mathcal{B}(B \rightarrow X_{s+d}\gamma))}{(\mathcal{B}(\bar{B} \rightarrow X_{s+d}\gamma) + \mathcal{B}(B \rightarrow X_{s+d}\gamma))}. \quad (4)$$

We tag the B flavor by the lepton charge. Using a sample 384×10^6 $B\bar{B}$ events, we measure $\mathcal{A}_{CP}(B \rightarrow X_{s+d}\gamma) = 0.057 \pm 0.06_{stat} \pm 0.018_{sys}$ after correcting for charge bias and mistagging [8]. Figure 6 shows all \mathcal{A}_{CP} measurements from *BABAR* [8, 20, 22], *Belle* [25] and *CLEO* [15]. They all agree well with the SM prediction [27, 28].

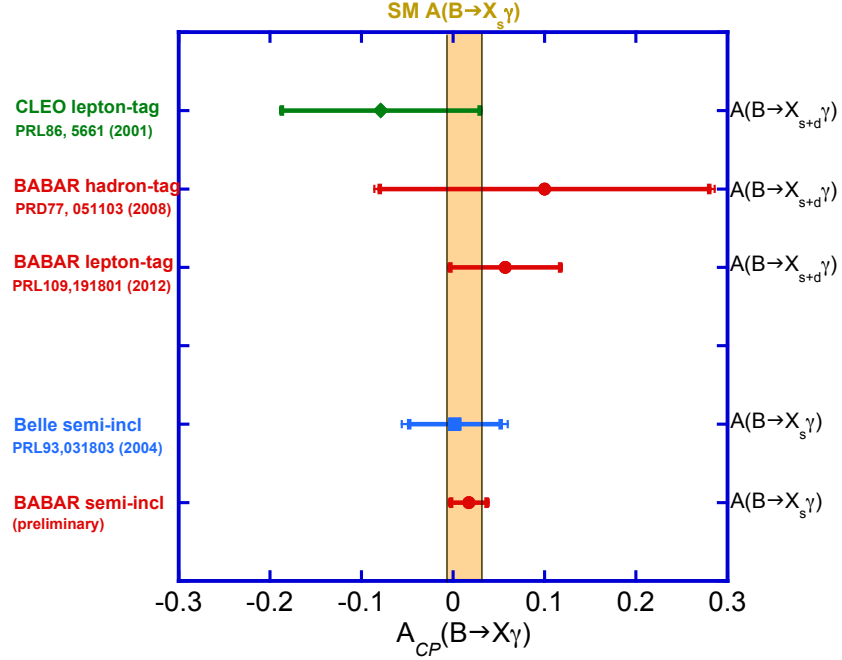


Figure 6: Summary of \mathcal{A}_{CP} measurements for $B \rightarrow X_s\gamma$ from semi-inclusive analyses (*BABAR* preliminary, *Belle* [25]) and for $B \rightarrow X_{s+d}\gamma$ from fully inclusive analyses (*BABAR* [8, 22] and *CLEO* [26]) in comparison to the SM prediction for $B \rightarrow X_s\gamma$ [24].

3 $B \rightarrow K^{(*)}\ell^+\ell^-$

Using 471 (657) $\times 10^6$ $B\bar{B}$ events, *BABAR* (*Belle*) reconstructs eight (ten) $B \rightarrow K^{(*)}\ell^+\ell^-$ final states consisting of $K^+, K_S^0, K^+\pi^-, K_S^0\pi^+, (K^+\pi^0)$ recoiling against e^+e^- or $\mu^+\mu^-$ [29, 30]. *BABAR* (*Belle*) selects e^\pm with momenta $p_e > 0.3$ (0.4) GeV/ c . Both experiments select muons with $p_\mu > 0.7$ GeV/ c , require good particle identification for e^\pm, μ^\pm, π^\pm and K^\pm and reconstruct K_S^0 in the $\pi^+\pi^-$ final state. To suppress combinatorial $q\bar{q}$ and $B\bar{B}$ backgrounds, *BABAR* uses eight boosted decision trees (BDT),[¶] while *Belle* uses likelihood ratios. Both experiments select signal with m_{ES} and ΔE and veto the J/ψ and $\psi(2S)$ mass regions. The vetoed J/ψ and $\psi(2S)$ samples and generated pseudo experiments are used to check the performance of the selection. To extract signal yields, both experiments perform one-dimensional fits of the m_{ES} distributions for $B \rightarrow K\ell^+\ell^-$ modes and two-dimensional fits of the m_{ES} and $m_{K\pi}$ mass distributions for $B \rightarrow K^*\ell^+\ell^-$ modes.

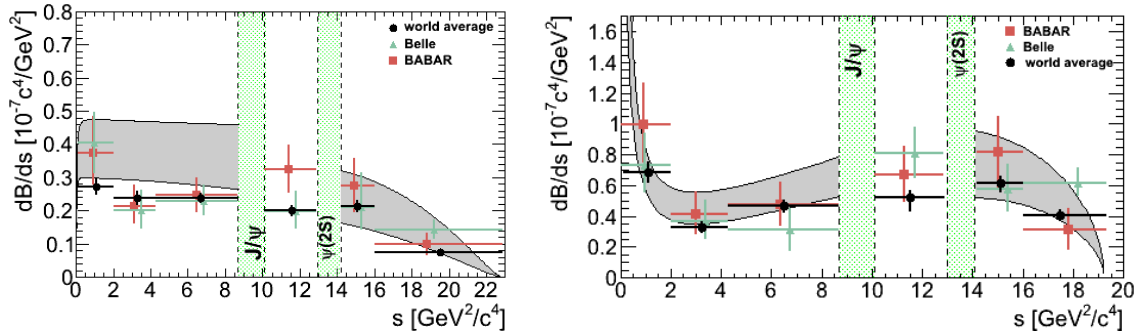


Figure 7: $d\mathcal{B}/ds$ measurements for $B \rightarrow K\ell^+\ell^-$ (left) and $B \rightarrow K^*\ell^+\ell^-$ (right) from *BABAR* [29] (red squares), *Belle* [30] (green triangles) and a naive world average (black points) that is dominated by LHCb in comparison to the SM predictions [38] (grey curves). Vertical bands show the J/ψ and $\psi(2S)$ vetoed regions.

3.1 $B \rightarrow K^{(*)}\ell^+\ell^-$ Rates and Rate Asymmetries

BABAR [29] and *Belle* [30] measured total and partial branching fractions $d\mathcal{B}(B \rightarrow K^{(*)}\ell^+\ell^-)/ds$ in six $s = q^2 = m_{\ell^+\ell^-}^2$ bins.^{||} Figure 7 (left) shows the *BABAR* and *Belle* $d\mathcal{B}(B \rightarrow K\ell^+\ell^-)/ds$ measurements in comparison to a naive average that includes the $B \rightarrow K\ell^+\ell^-$ modes from *BABAR* [29] and *Belle* [30] and $B \rightarrow K\mu^+\mu^-$ modes from CDF [31] and LHCb [32]. Figure 7 (right) shows the corresponding $d\mathcal{B}(B \rightarrow$

[¶]two BDTs are used to separate signal from $B\bar{B}$ and $q\bar{q}$ backgrounds, separately for e^+e^- and $\mu^+\mu^-$ modes and separately for s below and above the J/ψ mass.

^{||} q is the momentum transfer and $m_{\ell^+\ell^-}$ is the dilepton mass.

$K^*\ell^+\ell^-$)/ ds results. The average is calculated using $B \rightarrow K^*\ell^+\ell^-$ modes from BABAR [29] and Belle [30], $B \rightarrow K^*\mu^+\mu^-$ modes from CDF [31] and LHCb [33, 34] as well as the $B \rightarrow K^{*0}\mu^+\mu^-$ mode from CMS [35]. Note that the average values are dominated by the LHCb result. All measurements agree well with the SM predictions that are calculated for low and high values of s [36, 37, 38]. For low s , the hadronic recoil is large and the $K^{(*)}$ energy is much larger than the QCD scale Λ ($E_{K^{(*)}} \gg \Lambda$). This region represents the perturbative regime in which QCD factorization yields reliable results [39, 40]. For high $s \sim \mathcal{O}(m_b)$, the hadronic recoil becomes small and $E_{K^{(*)}} \sim \Lambda$. This is the non-perturbative regime in which an operator product expansion in powers of $1/m_b$ yields reliable results. The large uncertainties in the SM predictions result from the uncertainties in calculating the form factors of the hadronic matrix elements [41].

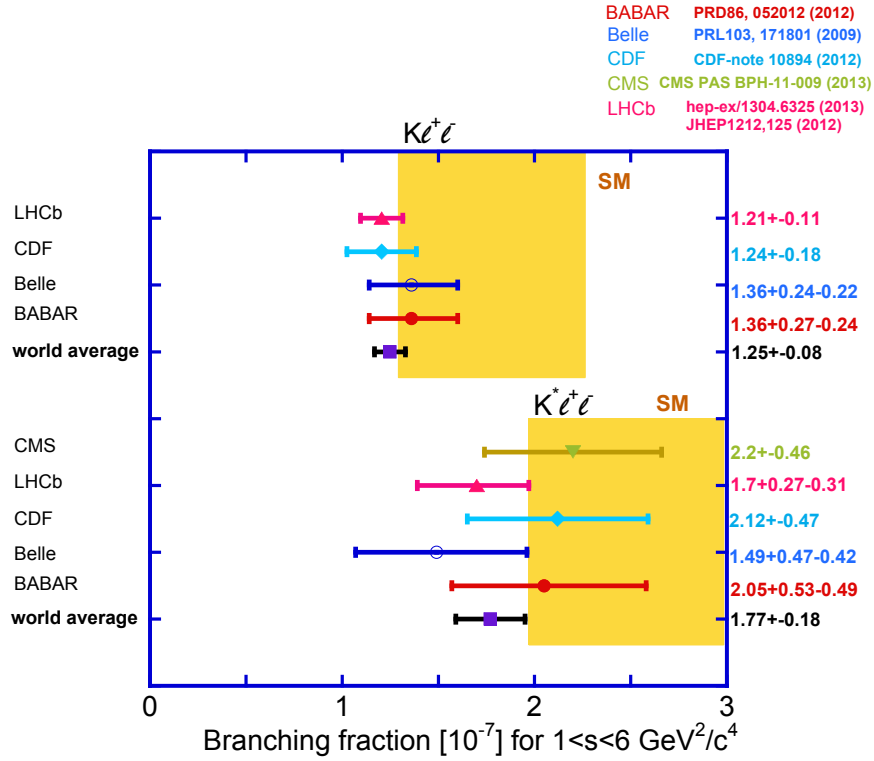


Figure 8: Branching fraction measurements for $B \rightarrow K\ell^+\ell^-$ and $B \rightarrow K^*\ell^+\ell^-$ in the low s region ($1 < s < 6 \text{ GeV}/c^2$) from BABAR [29], Belle [30], CDF [31], LHCb [32, 34] and CMS [35] in comparison to the SM predictions [38].

Figure 8 shows all $B \rightarrow K\ell^+\ell^-$ and $B \rightarrow K^*\ell^+\ell^-$ branching fractions measured in the low s region, $1 < s < 6 \text{ GeV}/c^2$, in comparison to SM predictions [38]. Figure 9 shows $B \rightarrow K^{(*)}\ell^+\ell^-$ total branching fraction measurements in comparison to SM

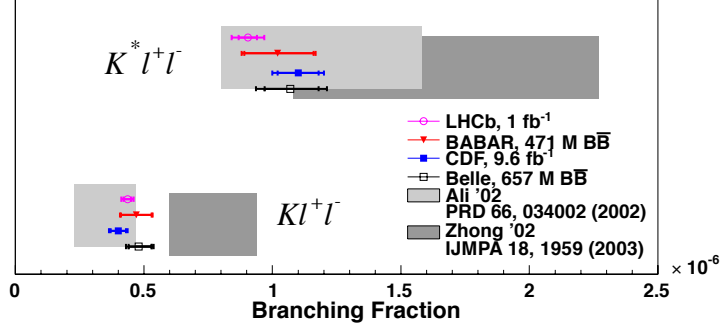


Figure 9: Total branching fraction measurements for $B \rightarrow K\ell^+\ell^-$ and $B \rightarrow K^*\ell^+\ell^-$ from *BABAR* [20], Belle [30], CDF [31] and LHCb [32, 34] in comparison to the SM predictions [42, 43].

predictions [42, 43]. All measurements show better agreement with the Ali model [42]. *BABAR* measured total branching fractions of $\mathcal{B}(B \rightarrow K\ell^+\ell^-) = (4.7 \pm 0.6_{stat} \pm 0.2_{sys}) \times 10^{-7}$ and $\mathcal{B}(B \rightarrow K^*\ell^+\ell^-) = (10.2^{+1.4}_{-1.3}{}_{stat} \pm 0.5_{sys}) \times 10^{-7}$. Table 2 summarizes the *BABAR* total branching fraction and rate asymmetry measurements.

The isospin asymmetry is defined by

$$d\mathcal{A}_I/ds \equiv \frac{d\mathcal{B}(B^0 \rightarrow K^{(*)0}\ell^+\ell^-)/ds - r_\tau d\mathcal{B}(B^+ \rightarrow K^{(*)+}\ell^+\ell^-)/ds}{d\mathcal{B}(B^0 \rightarrow K^{(*)0}\ell^+\ell^-)/ds + r_\tau d\mathcal{B}(B^+ \rightarrow K^{(*)+}\ell^+\ell^-)/ds}, \quad (5)$$

where $r_\tau = \tau_{B^0}/\tau_{B^+}$ accounts for the different B^0 and B^+ lifetimes. In the SM, \mathcal{A}_I is expected to be at the order of $\mathcal{O}(1\%)$ [44].

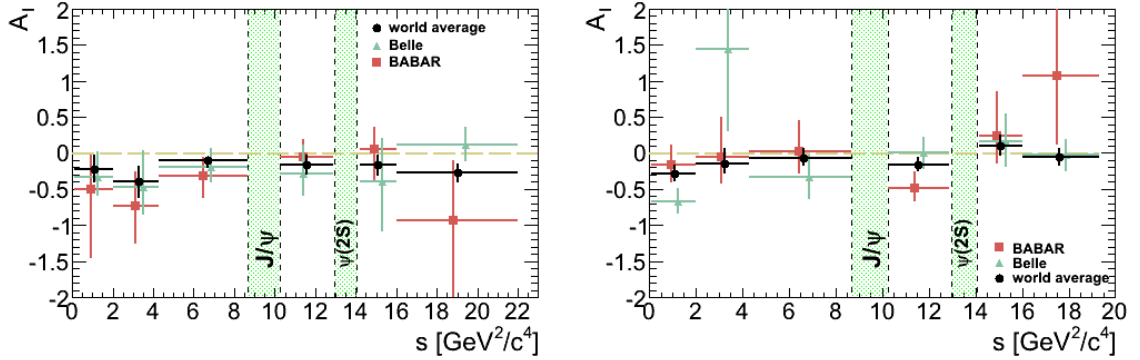


Figure 10: Isospin asymmetry for $B \rightarrow K\ell^+\ell^-$ (left) and $B \rightarrow K^*\ell^+\ell^-$ (right) for *BABAR* [20] (red squares), Belle [30] (green triangles) and a naive world average over all experiments (black points) that is dominated by LHCb. Vertical bands show the J/ψ and $\psi(2S)$ vetoed regions. The dashed line indicates the SM prediction [44].

Table 2: *BABAR* results for $B \rightarrow K^{(*)}\ell^+\ell^-$ modes on total branching fractions, CP asymmetries, lepton flavor ratios and isospin asymmetries. The first uncertainty is statistical, the second is systematic.

Mode s [$\frac{\text{GeV}^2}{c^4}$]	$\mathcal{B}[10^{-7}]$ all s	\mathcal{A}_{CP} all s	$\mathcal{R}_{K^{(*)}}$ $s > 0.1 \text{ GeV}^2/c^4$	\mathcal{A}_I $0.1 \leq s \leq 8.12$
$K\ell^+\ell^-$	$4.7 \pm 0.6 \pm 0.2$	$-0.03 \pm 0.14 \pm 0.01$	$1.00^{+0.31}_{-0.25} \pm 0.07$	$-0.58^{+0.29}_{-0.37} \pm 0.02$
$K^*\ell^+\ell^-$	$10.2^{+1.4}_{-1.3} \pm 0.05$	$0.03 \pm 0.13 \pm 0.01$	$1.13^{+0.34}_{-0.26} \pm 0.10$	$-0.25^{+0.17}_{-0.20} \pm 0.03$

Figure 10 shows *BABAR* and Belle isospin asymmetry measurements in six s bins for $B \rightarrow K\ell^+\ell^-$ modes (left) and $B \rightarrow K^*\ell^+\ell^-$ modes (right) in comparison to a naive average over all experiments (*BABAR* [20], Belle [30], CDF [31], and LHCb [45]). The average points are dominated again by LHCb. At low s ($1 < s < 6 \text{ GeV}^2/c^2$), the naive average yields $\mathcal{A}_I^{low\ s}(B \rightarrow K\ell^+\ell^-) = -0.31 \pm 0.12$ and $\mathcal{A}_I^{low\ s}(B \rightarrow K^*\ell^+\ell^-) = -0.15 \pm 0.11$. For $B \rightarrow K\ell^+\ell^-$, consistency with the SM is at the $\sim 2.6\sigma$ level. For other s values and for $B \rightarrow K^*\ell^+\ell^-$, the averaged data agree well with the SM prediction [44]. The *BABAR* measurements are listed in Table 2.

The CP asymmetry is defined by

$$\mathcal{A}_{CP} = \frac{\mathcal{B}(\bar{B} \rightarrow \bar{K}^{(*)}\ell^+\ell^-) - \mathcal{B}(B \rightarrow K^{(*)}\ell^+\ell^-)}{\mathcal{B}(\bar{B} \rightarrow \bar{K}^{(*)}\ell^+\ell^-) + \mathcal{B}(B \rightarrow K^{(*)}\ell^+\ell^-)}. \quad (6)$$

In the SM, the CP asymmetry is expected to be small, $\mathcal{A}_{CP} = -0.01$ [47, 48]. The measurements from *BABAR* [8] (see Table 2), Belle [14] and LHCb [46] agree well with the SM prediction.

The lepton flavor ratios are defined by

$$\mathcal{R}_{K^{(*)}} = \mathcal{B}(B \rightarrow K^{(*)}\mu^+\mu^-)/\mathcal{B}(B \rightarrow K^{(*)}e^+e^-). \quad (7)$$

In the SM for $s > 4m_\mu^{2,**}$ $\mathcal{R}_K^{(*)} \equiv 1$ [50]. For $s > 0.1 \text{ GeV}^2/c^4$, *BABAR* [8] (see Table 2) and Belle [14] measure lepton flavor ratios that are consistent with unity and thus agree well with the SM prediction.

Except for $\mathcal{A}_I(B \rightarrow K\ell^+\ell^-)$ at low s , all other measurements of branching fractions and rate asymmetries are in good agreement with the SM predictions.

3.2 $B \rightarrow K^{(*)}\ell^+\ell^-$ Angular Analyses

The $B \rightarrow K^*\ell^+\ell^-$ decay is characterized by three angles: θ_K is the angle between the K and B in the K^* rest frame, θ_ℓ is the angle between the ℓ^+ and the B in the

** m_μ is the muon mass.

$\ell^+\ell^-$ rest frame and ϕ is the angle between the K^* and $\ell^+\ell^-$ decay planes. The one-dimensional $\cos\theta_K$ and $\cos\theta_\ell$ projections depend on the K^* longitudinal polarization \mathcal{F}_L and the lepton forward-backward asymmetry \mathcal{A}_{FB} [50, 51]

$$\begin{aligned} W(\cos\theta_K) &= \frac{3}{2}\mathcal{F}_L \cos^2\theta_K + \frac{3}{4}(1 - \mathcal{F}_L) \sin^2\theta_K, \\ W(\cos\theta_\ell) &= \frac{3}{4}\mathcal{F}_L \sin^2\theta_\ell + \frac{3}{8}(1 - \mathcal{F}_L)(1 + \cos^2\theta_\ell) + \mathcal{A}_{FB} \cos\theta_\ell. \end{aligned} \quad (8)$$

In the SM, \mathcal{A}_{FB} and \mathcal{F}_L are again calculated separately for the low s and high s regions.

Since the number of signal events in each s bin is small, *BABAR* and Belle analyze one-dimensional angular distributions. Using 471 $B\bar{B}$ events, *BABAR* reconstructs six $B \rightarrow K^*\ell^+\ell^-$ final states with $K^* \rightarrow K^+\pi^-, K_S^0\pi^+, K^+\pi^0$. The event selection is similar to that for rate asymmetries. *BABAR* extracts \mathcal{F}_L and \mathcal{A}_{FB} by performing a profile likelihood scan. Using 657 $B\bar{B}$ events, Belle performs a fit to the one-dimensional angular distributions.

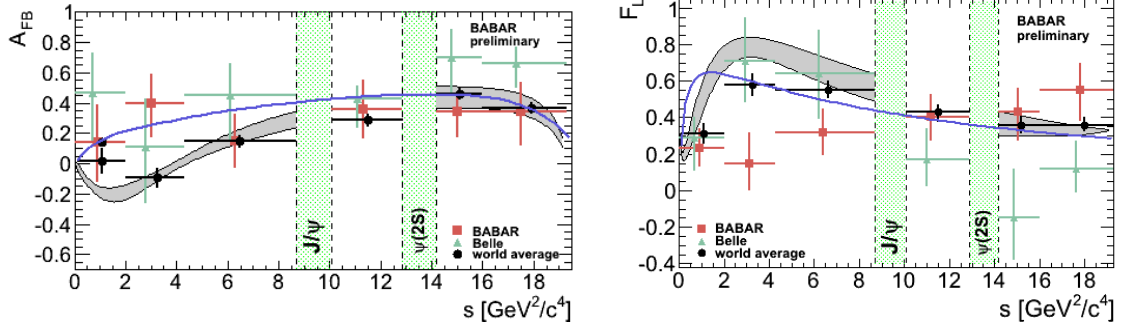


Figure 11: *BABAR* preliminary measurements (red squares) and Belle results [30] (green triangles) for \mathcal{A}_{FB} (left) and \mathcal{F}_L (right) for $B \rightarrow K^*\ell^+\ell^-$ modes in comparison to the naive world average over all experiments (black points) that is dominated by LHCb, the SM prediction (shaded curves) and a model in which the sign of C_7^{eff} is flipped (blue solid curve). Vertical bands show the J/ψ and $\psi(2S)$ vetoed regions.

Figure 11 (left) shows \mathcal{A}_{FB} measurements in six s bins from *BABAR* (preliminary) and Belle [30] in comparison to a naive average over the $B \rightarrow K^*\ell^+\ell^-$ results from *BABAR* and Belle [30], $B \rightarrow K^*\mu^+\mu^-$ results from CDF [31] and $B \rightarrow K^{*0}\mu^+\mu^-$ results from LHCb [34], CMS [35] and ATLAS [49]. The average values are dominated again by the LHCb measurements. In addition, predictions are shown for the SM and for a model in which the sign of Wilson coefficient C_7^{eff} is flipped with respect to the expected value in the SM [42, 47, 50, 53]. The large uncertainties in the SM predictions result from uncertainties in the form factor calculations. While the *BABAR*

Table 3: *BABAR* measurements of the lepton forward-backward asymmetry and K^* longitudinal polarization for $B \rightarrow K^*\ell^+\ell^-$ modes in the low s region. The first uncertainty is statistical, the second is systematic.

Mode	\mathcal{A}_{FB}	\mathcal{F}_L
s [$\frac{\text{GeV}^2}{c^4}$]	$1.0 \leq s \leq 6.0$	$1.0 \leq s \leq 6.0$
$K^*\ell^+\ell^-$	$0.26^{+0.27}_{-0.30} \pm 0.07$	$0.25^{+0.09}_{-0.08} \pm 0.03$

measurements are consistent with both the SM and the flipped-sign C_7^{eff} model, the world average values agree well with the SM prediction. In the low s region, the world average yields $\mathcal{A}_{FB}(B \rightarrow K^*\ell^+\ell^-) = -0.074^{+0.047}_{-0.048}$, which agrees well with the SM prediction of $\mathcal{A}_{FB}^{SM}(B \rightarrow K^*\ell^+\ell^-) = -0.0494^{+0.0281}_{-0.0252}$ (for *BABAR* results see Table 3).

Figure 11 (right) shows \mathcal{F}_L measurements from *BABAR* (preliminary) and Belle [30] in six s bins in comparison to a naive average using $B \rightarrow K^*\ell^+\ell^-$ results from *BABAR* and Belle [30], $B \rightarrow K^*\mu^+\mu^-$ results from CDF [31] and $B \rightarrow K^{*0}\mu^+\mu^-$ results from LHCb [34], CMS [35] and ATLAS [49]. The naive average values are again dominated by the LHCb results. The figure also shows the SM prediction [38] and the prediction of the flipped-sign C_7^{eff} model [42, 47, 50]. All results are consistent with the SM prediction, though the *BABAR* results fit better to the flipped-sign C_7^{eff} model. In the low s region ($1 < s < 6 \text{ GeV}^2/c^4$), the world average yields $\mathcal{F}_L(B \rightarrow K^*\ell^+\ell^-) = 0.523^{+0.047}_{-0.044}$, which is consistent with the SM prediction of $\mathcal{F}_L^{SM}(B \rightarrow K^*\ell^+\ell^-) = 0.735^{+0.06}_{-0.07}$ [38, 47, 50, 52, 53] (for *BABAR* results see Table 3).

4 Search for $B \rightarrow \pi\ell^+\ell^-$ and $B \rightarrow \eta\ell^+\ell^-$ Decays

In the SM in lowest order, $B \rightarrow X_d\ell^+\ell^-$ modes are also mediated by the electromagnetic penguin, Z penguin and WW box diagrams. However, they are suppressed by $|V_{td}/V_{ts}|^2 \sim 0.04$ with respect to the corresponding $B \rightarrow X_s\ell^+\ell^-$ modes. In extensions of the SM, rates may increase significantly [54]. Using $471 \times 10^6 B\bar{B}$ events, *BABAR* recently updated the search for $B \rightarrow \pi\ell^+\ell^-$ modes and performed the first search for $B \rightarrow \eta\ell^+\ell^-$ modes. The SM predictions lie in the range $\mathcal{B}(B \rightarrow \pi\ell^+\ell^-) = (1.96 - 3.30) \times 10^{-8}$ and $\mathcal{B}(B \rightarrow \eta\ell^+\ell^-) = (2.5 - 3.7) \times 10^{-8}$ where the large uncertainties result from uncertainties in the $B \rightarrow \pi$ form factor calculations [54, 55, 56] and from a lack of knowledge of $B \rightarrow \eta$ form factors [57].

BABAR fully reconstructs four $B \rightarrow \pi\ell^+\ell^-$ and four $B \rightarrow \eta\ell^+\ell^-$ final states by selecting $\pi^\pm, \pi^0, \eta \rightarrow \gamma\gamma$ and $\eta \rightarrow \pi^+\pi^-\pi^0$ recoiling against e^+e^- or $\mu^+\mu^-$ [58]. We select leptons with $p_\ell > 0.3 \text{ GeV}/c$, recover losses due to bremsstrahlung for e^\pm , remove $\gamma \rightarrow e^+e^-$ decays and require good particle identification for e^\pm, μ^\pm and

π^\pm . We select photons with $E_\gamma > 50$ MeV and impose a π^0 mass constraint of $115 < m_{\gamma\gamma} < 150$ MeV/ c^2 and an η mass constraint of 500 (535) $< m_{\gamma\gamma}$ ($m_{3\pi}$) < 575 (565) MeV/ c^2 . In addition, we require $(E_{1,\gamma} - E_{2,\gamma})/(E_{1,\gamma} + E_{2,\gamma}) < 0.8$ for the $\eta \rightarrow \gamma\gamma$ final states to remove asymmetric $q\bar{q}$ background that peaks near one. We veto J/ψ and $\psi(2S)$ mass regions and use four NNs to suppress combinatorial $B\bar{B}$ and $q\bar{q}$ continuum backgrounds, separately for e^+e^- modes and for $\mu^+\mu^-$ modes. The NNs for suppressing $B\bar{B}$ background uses 15 (14) input distributions for e^+e^- ($\mu^+\mu^-$) modes, while those for suppressing $q\bar{q}$ continuum use 16 input distributions for both modes. For validations, we use pseudo-experiments and the vetoed J/ψ and $\psi(2S)$ samples. The selection criteria used by Belle are given in [59].

For $B \rightarrow \pi^+\ell^+\ell^-$ and $B \rightarrow \pi^0\ell^+\ell^-$, BABAR performs simultaneous unbinned maximum likelihood fits to the m_{ES} and ΔE distributions for e^+e^- and $\mu^+\mu^-$ modes separately. We include the $B \rightarrow K^+\ell^+\ell^-$ mode in the fit to extract the peaking background contribution in the $B \rightarrow \pi^+\ell^+\ell^-$ modes by reconstructing the K^+ as a π^+ . We use the vetoed J/ψ and $\psi(2S)$ samples to validate the fit and check the peaking $B \rightarrow K^+\ell^+\ell^-$ contribution.

For the $B \rightarrow \eta\ell^+\ell^-$, we perform simultaneous unbinned maximum likelihood fits to the m_{ES} and ΔE distributions, again for e^+e^- and $\mu^+\mu^-$ modes separately. We use the vetoed J/ψ and $\psi(2S)$ samples to validate the fits. In addition, we perform fits for the isospin-averaged modes $B \rightarrow \pi e^+e^-$ and $B \rightarrow \pi\mu^+\mu^-$, lepton-flavor averaged modes $B^+ \rightarrow \pi^+\ell^+\ell^-$, $B^0 \rightarrow \pi^0\ell^+\ell^-$ and $B^0 \rightarrow \eta\ell^+\ell^-$ and both isospin and lepton-flavor averaged modes $B \rightarrow \pi\ell^+\ell^-$.

Similar to Belle, we see no signals in any of these modes and set branching fraction upper limits at 90% CL. Recently, LHCb observed the $B \rightarrow \pi^+\ell^+\ell^-$ decay and measured a branching fraction of $\mathcal{B}(B \rightarrow \pi^+\ell^+\ell^-) = (2.4 \pm 0.6 \pm 0.1) \times 10^{-8}$ [60]. Figure 12 shows the preliminary BABAR branching fraction upper limits in comparison to those from Belle [59] and the $B \rightarrow \pi^+\ell^+\ell^-$ measurement from LHCb [60]. BABAR sets the best branching fraction upper limit for $B^0 \rightarrow \pi^0\ell^+\ell^-$ and presents the first results for $B \rightarrow \eta\ell^+\ell^-$ modes. Note that the present branching fraction upper limits lie within a factor of two to three of the SM predictions.

5 Conclusion

The BABAR $B \rightarrow X_s\gamma$ measurements of branching fractions, photon energy moments, m_b , μ_π^2 are in good agreement with the SM predictions. The $\mathcal{B}(B \rightarrow X_s\gamma)$ measurement provides a constraint on the charged Higgs mass of $M_{H^\pm} > 327$ GeV/ c^2 at 95% CL independent of $\tan\beta$. The new $\mathcal{A}_{CP}(B \rightarrow X_s\gamma)$ measurement is the most precise result and agrees well with the SM prediction. The BABAR $\Delta\mathcal{A}_{CP}(B \rightarrow X_s\gamma)$ measurement is the first one and provides the first constraint on $\mathcal{I}m(C_8^{eff}/C_7^{eff})$. BABAR updated branching fraction upper limits for $B \rightarrow \pi\ell^+\ell^-$ and presented the

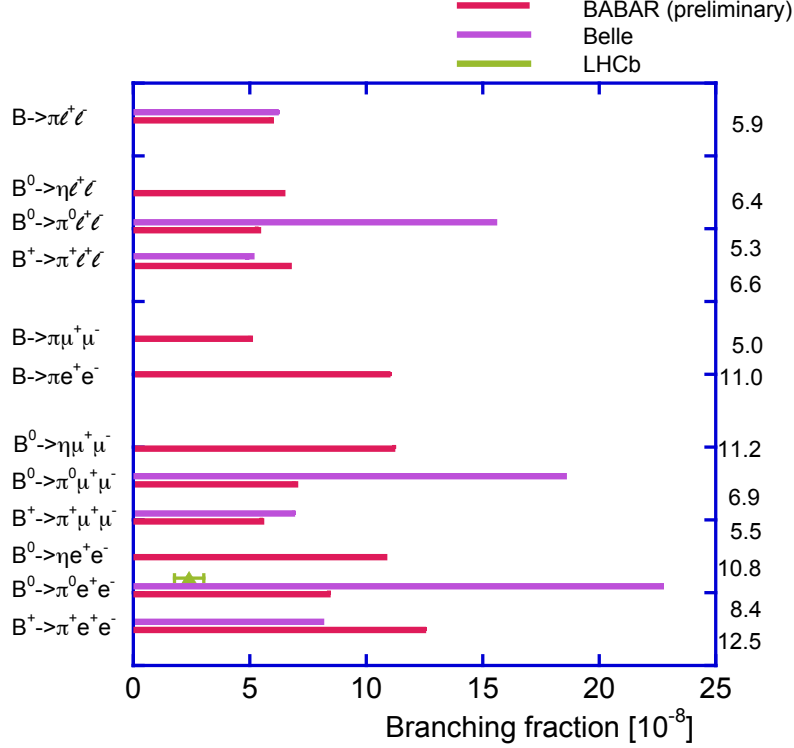


Figure 12: Branching fraction upper limits at 90% CL for $B \rightarrow \pi \ell^+ \ell^-$ and $B \rightarrow \eta \ell^+ \ell^-$ modes from *BABAR* (preliminary) and Belle [59] and the measurement of $B \rightarrow \pi^+ \ell^+ \ell^-$ by LHCb [60].

first branching fraction upper limits for $B \rightarrow \eta \ell^+ \ell^-$.

For $B \rightarrow K^{(*)} \ell^+ \ell^-$, the measurements of branching fractions, isospin asymmetries, lepton flavor ratios, CP asymmetries, K^* longitudinal polarization and lepton forward-backward asymmetry averaged over all experiments agree with the SM predictions. The largest deviation from the SM prediction is less than 3σ and results from the isospin asymmetry of $B \rightarrow K \ell^+ \ell^-$ in the low s region. To look for more deviations from the SM, the precision of all measurements needs to be improved significantly. Such improvements are expected to come from LHCb and Belle II. Furthermore, large data samples in these experiments will permit studies of the full angular distribution in $B \rightarrow K^* \ell^+ \ell^-$, which is described by 12 observables [61, 62]. Some the new observables have a higher discrimination power between the SM and new physics effects \mathcal{A}_{FB} and \mathcal{F}_L .

ACKNOWLEDGEMENTS

I would like to thank members of the *BABAR* collaboration for giving me the opportunity to present these results. In particular, I would like to thank Piti Ongmongkolkul, Bill Dunwoodie, David Hitlin and Jack Ritchie for their fruitful suggestions. Furthermore, I would like to thank Gudrun Hiller and Aoife Bharucha for supplying Mathematica files with the SM predictions for $B \rightarrow K^{(*)}\ell^+\ell^-$ modes.

References

- [1] K. Wilson, Phys. Rev. **179**, 1499 (1969); K. Wilson and J. Kogut, Phys. Rep. **12**, 75 (1974).
- [2] N. Isgur *et al.* Phys.Rev. D **39**, 799 (1989); N. Isgur and M. Wise, Phys. Lett. B **232**, 113 (1989).
- [3] H. Georgi, Phys. Lett. B **240**, 447 (1990).
- [4] B. Grinstein and D. Pirjol, Phys. Rev. D **70**, 114005 (2004); arXiv:0404250 [hep-ph].
- [5] M. Misiak *et al.*, Phys. Rev. Lett. **98**, 022002 (2007); arXiv:0609232 [hep-ph].
- [6] M. Misiak and M. Steinhauser, Nucl. Phys.**B764**, 62 (2007); arXiv: 0609241[hep-ph].
- [7] M. Misiak, talk presented this conference, see proceedings (2013).
- [8] J.P Lees *et al.* (*BABAR* collaboration), Phys. Rev. Lett. **109**, 191801 (2012); arXiv:1207.2690 [hep-ex].
- [9] J.P Lees *et al.* (*BABAR* collaboration), Phys. Rev. D **86**, 112008 (2012); arXiv:1207.5772 [hep-ex].
- [10] D. Benson, I. Bigi and N. Uraltsev, Nucl. Phys. B **710**, 726 371 (2005); arXiv:0410080 [hep-ph].
- [11] M. Neubert, Phys. Rev. D **72**, 074025 (2005); arXiv:0506245 [hep-ph].
- [12] D. Asner *et al.*, arXiv:1010.1589v3 (2011); www.slac.stanford.edu/xorg/hfag/triangle/index.html (2013).
- [13] B. Aubert *et al.* (*BABAR* collaboration), Phys. Rev. D **72**, 052004 (2005); arXiv:0508004 [hep-ex].

- [14] A. Limosani *et al.* (Belle collaboration), Phys. Rev. Lett. **103**, 241801 (2009); arXiv:0907.1384 [hep-ex].
- [15] S. Chen *et al.* (CLEO collaboration), Phys. Rev. Lett. **87**, 251807 (2001); arXiv: 0108032 [hep-ex].
- [16] U. Haisch, arXiv:0805.2141 [hep-ph].
- [17] M. Ciuchini *et al.*, Nucl. Phys. B **527**, 21 (1998), arXiv:9710335 [hep-ph].
- [18] J.P Lees *et al.* (BABAR collaboration), Phys. Rev. Lett. **109**, 101802 (2013); arXiv: 1205.5442 [hep-ex].
- [19] J.P Lees *et al.* (BABAR collaboration), arXiv: 1303.0571 [hep-ex].
- [20] J.P Lees *et al.* (BABAR collaboration), Phys.Rev. D **86**, 052012 (2012); arXiv:1207.2520 [hep-ex].
- [21] B. Lange, M. Neubert and G. Paz, Phys. Rev. D **72**, 073006 (2005); arXiv:0504071 [hep-ph].
- [22] B. Aubert *et al.* (BABAR collaboration), Phys. Rev. D **77**, 051103 (2008); arXiv:0711.4889 [hep-ex].
- [23] K. Abe *et al.* (Belle collaboration), Phys. Lett. B **511**, 151 (2001); arXiv:0103042 [hep-ex].
- [24] M. Benzke *et al.*, Phys. Rev. Lett **106**, 141801 (2011); arXiv: 1012.3167 [hep-ph].
- [25] S. Nishida *et al.* (Belle collaboration), Phys. Rev. Lett. **93**, 031803 (2004); arXiv:0308038 [hep-ex].
- [26] T. E. Coan *et al.*, Phys.Rev. Lett. **86**, 5661 (2001); arXiv:0010075 [hep-ex].
- [27] A.L. Kagan and M. Neubert, Phys. Rev. D **58**, 094012 (1998), arXiv: 9803368 [hep-ph].
- [28] T. Hurth, E. Lunghi, and W. Porod, Phys. Rev. Lett. **106**, 141801 (2011); arXiv:1012.3167 [hep-ph].
- [29] J.P Lees *et al.* (BABAR collaboration), Phys.Rev. D **86**, 032012 (2012); arXiv:1204.3933 [hep-ex].
- [30] J. T. Wei *et al.* (Belle collaboration), Phys. Rev. Lett. **103**, 171801 (2009), arXiv: 0904.0770 [hep-ex].

- [31] T. Aaltonen *et al.* (CDF collaboration), CDF-note 10894 (2012); T. Aaltonen *et al.* (CDF collaboration), Phys. Rev. Lett. **108**, 081807 (2012); arXiv:1108.0695 [hep-ex].
- [32] R. Aaij *et al.* (LHCb collaboration), JHEP **1302**, 105 (2013); arXiv:1209.4284 [hep-ex].
- [33] R. Aaij *et al.* (LHCb collaboration), Phys. Rev. Lett. **108**, 181806 (2012); arXiv:1111.3515 [hep-ex].
- [34] R. Aaij *et al.* (LHCb collaboration), arXiv: 1304.6325 [hep-ex].
- [35] S. Chatrchyan *et al.* (CMS collaboration), arXiv: 1308.3409 [hep-ex].
- [36] C. Bobeth, G. Hiller and D. van Dyk, JHEP **1007**, 098 (2010); arXiv: 1006.5013 [hep-ph]; *ibid*, JHEP **1107**, 67 (2011); arXiv:1105.0376 [hep-ph].
- [37] C. Bobeth, G. Hiller and D. van Dyk,, JHEP **1201**, 107 (2013); arXiv:1111.2558 [hep-ph].
- [38] C. Bobeth, G. Hiller and D. van Dyk, Phys. Rev. D **8**, 034016 (2013); arXiv:1212.2321 [hep-ph].
- [39] M. Beneke, T. Feldmann and D. Seidel, Nucl. Phys. B **612**, 25 (2001); arXiv: 0106067 [hep-ph].
- [40] M. Beneke, T. Feldmann and D. Seidel, Eur. Phys. J. C **41**, 173 (2005); arXiv: 0412400 [hep-ph].
- [41] P. Ball and Zwicky, Phys. Rev. D **71**, 014015 (2005); arXiv: 0406232 [hep-ph] (2004); Phys. Rev. D **71**, 014029 (2005); arXiv: 0412079 [hep-ph].
- [42] A. Ali *et al.*, Phys. Rev. D **66**, 034002 (2002); arXiv: 0112300 [hep-ph].
- [43] M. Zhong, Y.L. Wu and W.Y. Wang, Int.J.Mod.Phys. A **18**, 1959 (2003); arXiv: 0206013 [hep-ph].
- [44] Th. Feldmann and J. Matias, JHEP **301**, 074 (2003), arXiv: 0212158 [hep-ph].
- [45] R. Aaij *et al.* (LHCb collaboration), JHEP **1207**, 133 (2012); arXiv:1205.3422 [hep-ex].
- [46] R. Aaij *et al.* (LHCb collaboration), Phys. Rev. Lett. **110**, 031801 (2012); arXiv:1210.4492 [hep-ex].
- [47] F. Krüger *et al.*, Phys. Rev. D **61**, 114028 (2000); Erratum-*ibid.* D **63**, 019901 (2001); arXiv: 9907386 [hep-ph].

- [48] C. Bobeth, G. Hiller and G. Piranishvili, JHEP **0807**, 106 (2008); arXiv: 0805.2525 [hep-ph].
- [49] G. Aad *et al.* (ATLAS collaboration), ATLAS-CONF-2013-038 (2013).
- [50] A. Ali *et al.*, Phys. Rev. D **61**, 074024 (2000); arXiv: 9910221 [hep-ph] (1999).
- [51] C. Bobeth *et al.*, JHEP **0712**, 040 (2007); arXiv:0709.4174 [hep-ph].
- [52] F. Krüger and J. Matias, Phys. Rev. D **71**, 094009 (2005); arXiv: 0502060 [hep-ph].
- [53] G. Buchalla *et al.*, Phys. Rev. D **63**, 014015 (2000); arXiv: 0006136 [hep-ph].
- [54] T. M. Aliev and M. Savci, Phys. Rev. D **60**, 014005 (1999); arXiv: hep-ph/9812272 [hep-ph].
- [55] J. J. Wang, *et al.*, Phys. Rev. D **77**, 014017 (2008); arXiv:0711.0321 [hep-ph].
- [56] H. Z. Song, L. X. Lu, and G. R. Lu, Commun. Theor. Phys. **50**, 696 (2008).
- [57] G. Erkol and G. Turan, Eur. Phys. Jour. C **28**, 243 (2003); arXiv: 0212079 [hep-ph].
- [58] J.P Lees *et al.* (BABAR collaboration), arXiv: 1303.6010 [hep-ex].
- [59] J.T. Wei *et al.*, Phys. Rev. D **78**, 011101 (2008); arXiv:0804.3656 [hep-ex] .
- [60] R. Aaij *et al.* (LHCb collaboration), JHEP **1212**, 125 (2012); arXiv:1210.1089 [hep-ex].
- [61] W. Altmannshofer *et al.*, JHEP **0901**, 019 (2009); arXiv:0811.1214 [hep-ph].
- [62] U. Egede *et al.*, JHEP **1010**, 056 (2010); arXiv:1005.0571 [hep-ph] .